New metamaterial structure with reconfigurable refractive index at 5G candidate band

B. A. F. ESMAIL[a], H. A. MAJID[a], Z. Z. ABIDIN[a], S. H. DAHLAN[a], M. K. A. RAHIM[b], O. AYOP[b]
[a] *Applied Electromagnetics Center, Universiti Tun Hussein Onn Malaysia, 86400 Parit Raja, Batu Pahat, Johor, Malaysia*
[b] *Faculty of Electrical Engineering, Universiti Teknologi Malaysia, 81310 Skudai, Johor, Malaysia*

A new metamaterial structure with a reconfigurable refractive index for beam tilting in future fifth-generation (5G) networks has been designed and numerically investigated. The novel structure operates at 28 GHz and consists of a stairway-shaped resonator (SSR) printed on the top view of the substrate layer. The inductance and capacitance (LC) equivalent circuit model is introduced to estimate the electromagnetic behavior of the SSR unit cell. The circuit model data agreed well with the full-wave computer simulation technology (CST) simulation. The proper configuration of the SSR unit cell offers a very low loss of –0.26 dB. To control the refractive index of the proposed structure, two active components, PIN diodes, are formed in the gaps of the structure. Consequently, the SSR can be switched between four states with different refractive index values, which are –60, –14, 0, and –12 (Nicolson Ross Weir (NRW) method) and -58, -12.5, 1, and -10.4 (Robust Retrieval Method (RRM)) at 28 GHz. The return loss, insertion loss, and real parts of the refractive index are studied and investigated at each reconfigurable state. The copper strip and the measured S-parameters of the proposed PIN diode are used in the simulation to achieve reconfigurability.

(Received April 11, 2018; accepted February 12, 2019)

Keywords: 5G, Metamaterials, Negative refractive index, PIN diode, LC equivalent circuit

1. Introduction

Metamaterials are arrays of microstructure elements whose electromagnetic properties could be flexibly engineered. Unusual responses to electromagnetic indicate many noteworthy properties, such as negative refractive index and inverse Doppler shift, because of negative permittivity and permeability [1]. In 1967, the theoretical base of the unnatural physical properties of metamaterials was first introduced by Russian scientist Victor Veselago. However, these properties were hidden for 30 years, until Pendry verified them experimentally in 1996 [2], [3]. Recently, metamaterials have been extensively explored because of their numerous important applications; for example, they are used as perfect absorbers [4] and demonstrate the cloaking phenomenon [5]. Moreover, metamaterials were used for beam steering applications in the millimeter wave (MMW) band [6]. By loading metamaterials with a planar single-element antenna, the incident electromagnetic wave undergoes different refractive indexes and guides the antenna's main beam toward the desired direction.

Narrow bandwidth and losses are the main drawbacks of metamaterials, which affect the scope of their applications. At a high frequency range, such as MMW and terahertz bands, metamaterials suffer very high losses. The unnatural electromagnetic properties of metamaterials are negatively affected by these inherent losses [7]. Thus, a new low-loss metamaterial configuration is in high demand to enhance the performance of metamaterial devices, especially at a high frequency range. The tailoring geometry of the metamaterial configuration is the simplest and at the same time most effective method to overcome the inherent metamaterial losses [8]. In recent years, reconfigurable metamaterials have been a subject of interest for their potential to modify the electromagnetic properties of a metamaterial structure. Various methods, including mechanical, thermal, and electrical, have been proposed in the literature to tune the electromagnetic behavior of artificial structures [9]. The most common method is the electrical one, which has attracted considerable attention because of its potential to change the electromagnetic properties of metamaterials.

In this approach, the electrical switches such as the varactor diodes, PIN diodes, and microelectromechanical systems (MEMS), are formed in the structure to achieve reconfigurability. A varactor diode is a voltage-dependent capacitance and works in reverse bias. It has advantages, such as ease of installation and delivery, since it uses only a single diode to perform the reconfiguration. At a high-frequency range, a varactor diode with a tiny size that could be integrated into a very small metamaterial design is hard to find. Moreover, the variation in the capacitance values has little effect on the electromagnetic properties of the structure [10]. The best switch with high accuracy, low power, and low insertion loss is the MEMS switch; but this method has its own impairments, such as sophisticated manufacturing requirements, high cost, and delay in the tuning process, in comparison with other switches [9]. On the other hand, the PIN diode is represented as a variable resistance. This electrical switch offers special advantages over its active switch counterparts, such as

ease of installation, simple control, and fast tuning process [11], [12]. Furthermore, it is applicable to a high-frequency range.

In this work, a new refractive index reconfigurable low-loss metamaterial structure operating at 5G frequency band 28 GHz is designed and numerically investigated. Two PIN diodes are embedded in the new metamaterial structure to provide the reconfigurable feature. Three frequencies, F1 to F3, are created with different refractive index values based on two PIN diode states. Two methods, the copper strip and the measured S-parameters of the proposed PIN diode, are used to represent the PIN diode in the simulation. Moreover, the analytical model of the proposed structure is studied and investigated. The model merges an inductance and capacitance (LC) resonator with the existing analytic LC expressions. The analytical model agrees well with the full-wave simulations. Therefore, the proposed equivalent circuit model offers an alternative approach to accurately predict the resonance frequency of the proposed structure.

2. Design and simulation of the reconfigurable metamaterial structure

2.1. Metamaterial design

The design view of the proposed SSR structure is illustrated in Fig. 1. The SSR unit cell consists of two parallel strips of the copper layer joined together by a set of orthogonal strips printed on the front face of the substrate layer [13]. The inductance and capacitance effects are introduced by the square loops and gaps of the orthogonal strips, respectively. The proposed unit cell is printed on Rogers RT5880 with a thickness of 0.254 mm and a relative permittivity of 2.2. The unit cell specifications are described in the caption of Fig. 1. The metallic layer is a lossy metal copper with a thickness of 0.035 mm. To excite the electromagnetic wave and to extract the constitutive parameters, the ports and boundary conditions are assigned. The perfect magnetic conducting (PMC) and perfect electric conducting (PEC) boundary conditions are assigned along the x- and y-axis, respectively. The z-direction is used to guide the external electromagnetic wave. To achieve the reconfigurable refractive index property of the proposed metamaterial structure, two PIN diodes (D1 and D2) are formed in the gaps of the proposed SSR unit cell as shown in Fig. 1. The PIN diode is modeled as an adjustable resistance. The resistance of the PIN diode is determined only by a forward-biased DC current. When the PIN diode is forward-biased (ON state), the value of the resistance decreases close to 0 ohm. The PIN diode is reverse-biased (OFF state) and the resistance close to infinity. During forward bias, the PIN diode acts as a short circuit, whereas an open circuit is achieved when the PIN diode is reverse-biased. The MA4AGBL912 PIN diode is proposed in this work because of its wide operating frequency range up to 40 GHz.

2.2. Simulation methods

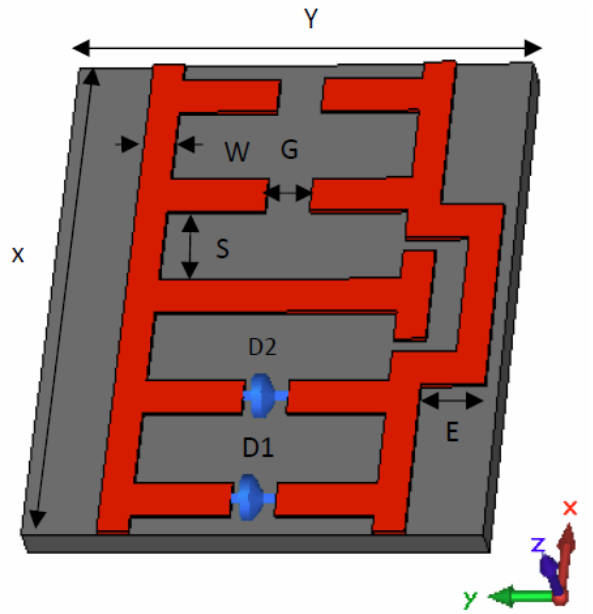

Fig. 1. (a) Schematic of the proposed reconfigurable metamaterial unit cell with dimensions in millimeters. X = 3.6, Y = 3.6, S = 0.65, E= 0.5, G = 0.35,G1 = 0.1 W = 0.25

Two methods are utilized here to represent the PIN in the simulation. The first method uses a copper strip to mimic the dimensions of the PIN. In this method, the ON state of the switch is represented by the copper strip, whereas vacuum represents the OFF state. The second method uses the measured S-parameters of the PIN diode during the simulation. In this method, the ON state is represented by the S-parameters of the proposed PIN diode, whereas the diode is left open in the OFF state. The S-parameters method in the full wave simulation is implemented through following steps:

Initially, place a discrete port at the position of the PIN diodes. Next, in the circuit simulation, external ports and a touchstone block are inserted and connected to the metamaterial block. The differential port needs to be set for the external ports and the metamaterial block. Fig. 2 shows the circuit simulation in CST when D1 and D2 are ON. The S-parameters of the PIN diode are set in the touchstone block. Waveguide ports 1 and 2 are used to feed the SSR structure, whereas ports 3 and 4 are the PIN diodes. Finally, the proposed structure is simulated using CST Microwave Studio based on the finite integration technique in the time domain solver. Due to the limitation of the S-parameters of the proposed PIN diode up to 30 GHz, two diodes are used to reconfigure the proposed unit cell. Furthermore, the PIN diodes have been placed close to each other therefore providing a minimum gap between reconfigured frequencies.

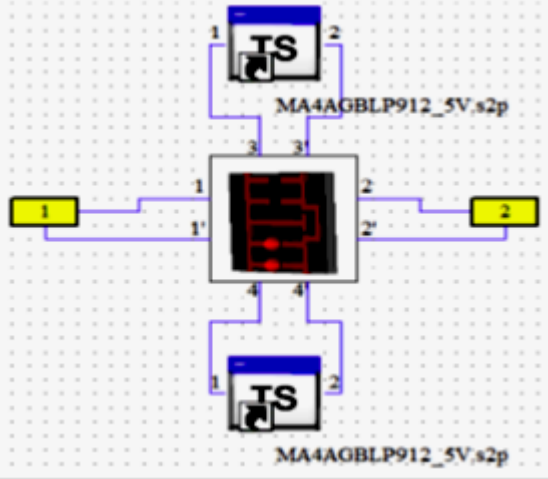

Fig. 2. Circuit simulation using CST software

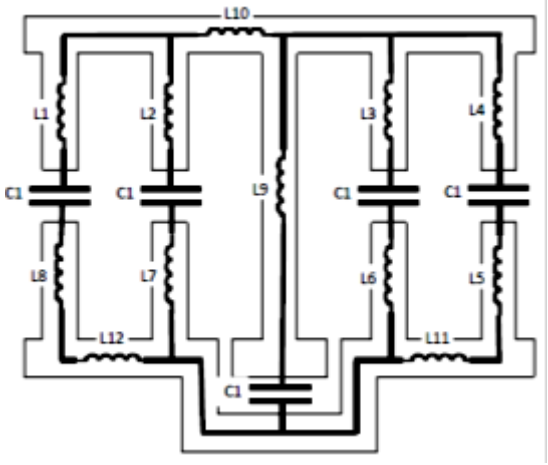

Fig. 3. LC equivalent circuit of the proposed SSR unit cell.

3. Equivalent circuit model of the SSR structure

In the literature, the electromagnetic behavior of metamaterial structures had been investigated theoretically, experimentally, or numerically using some full-wave electromagnetic solvers. These solvers, such as CST Microwave Studio or Ansoft's HFFS, usually require a very large computer memory space and need quite a long calculating time, especially with the periodic structures. Thus, the physical model is necessary to accurately predict the electromagnetic behavior of metamaterials in a simple, fast, and computationally efficient manner [14]. Moreover, the optimization approach in the design of metamaterial structures will be feasible. Furthermore, the availability of the equivalent circuit model introduces an easy way to establish the relationship between the parameter dimensions of the metamaterial structures and the frequency-dependent S-parameters behavior.

Several physical models had been proposed and studied in the literature, especially for the conventional split-ring resonator (SRR) structure, such as the RLC equivalent circuit model [14], [15], LC equivalent circuit model [15], and LMC equivalent circuit model [17], [18]. In this paper, the LC equivalent circuit is introduced and investigated to predict the S-parameters and constitutive parameters of the proposed SSR structure. Fig. 3 depicts the proposed LC equivalent circuit model which is introduced by five capacitances, represent the gaps of the proposed structure, and twelve inductances, represent the self-inductance of the conducting strips. All the geometrical parameters and material characteristics contribute to the model analysis, which is divided into self-inductance calculation and capacitance calculation.

The Bueno and Assis theory is utilized here to calculate the self-inductance of the conducting strips as follows [19], [17]:

$$\mathcal{L}(\ell_s, \omega_s) = \frac{\mu_0 \ell_s}{4\pi}\left[2\sinh^{-1}\left(\frac{\ell_s}{\omega_s}\right) + (1+t)\left(\frac{\ell_s}{\omega_s}\right)\sinh^{-1}\left(\frac{\omega_s}{\ell_s}\right) - \frac{(3-t)}{3}\frac{({\omega_s}^2+{\ell_s}^2)^{1.5}}{\ell_s {\omega_s}^2} + (1-t)\frac{\ell_s}{{\omega_s}^2}\left({\omega_s}^2+{\ell_s}^2\right)^{0.5} + \frac{2t}{3}\left(\frac{\ell_s}{\omega_s}\right)^2 + \frac{(3-t)}{3}\left(\frac{\omega_s}{\ell_s}\right)\right] \quad (1)$$

where ℓ_s and ω_s are the length and the width of the conducting strip, respectively. μ_0 is a free space permeability. t is an integer number and according to Neumann model, $t = 1$ [17]. Hence, Equation (1) is modified to:

$$\mathcal{L}(\ell_s, \omega_s) = \frac{\mu_0 \ell_s}{4\pi}\left[2\sinh^{-1}\left(\frac{\ell_s}{\omega_s}\right) + 2\left(\frac{\ell_s}{\omega_s}\right)\sinh^{-1}\left(\frac{\omega_s}{\ell_s}\right) - \frac{2}{3}\frac{({\omega_s}^2+{\ell_s}^2)^{1.5}}{\ell_s {\omega_s}^2} + \frac{2}{3}\left(\frac{\ell_s}{\omega_s}\right)^2 + \frac{2}{3}\left(\frac{\omega_s}{\ell_s}\right)\right] \quad (2)$$

L_1 through L_9 are the self-inductances of vertical conducting strips whereas L_{10}, L_{11}, and L_{12} are the self-inductance of horizontal conducting strips. The self-inductance of each conducting strip can be calculated as follows:

$L_1 = L_2 = L_3 = L_4 = L_5 = L_6 = L_7 = L_8 = \mathcal{L}(0.525\,, 0.25) = 218.8\text{pH}$, $L_9 = \mathcal{L}(2.9\,, 0.25) = 2.13\ \text{nH}$, $L_{10} = \mathcal{L}(2.24\,, 0.25) = 1.53\ \text{nH}$, and $L_{11} = L_{12} = \mathcal{L}(1.353\,, 0.25) = 0.8\ \text{pH}$.

The capacitances of the equivalent circuit model are calculated based on the partial capacitance method and line capacitance theory [20], [21]. The air gap capacitance and the capacitance of the substrate are separately calculated. Thereafter, both of them are combined to

compute the planar capacitor. The capacitance of the air gap layer is given by

$$\mathcal{C}_0 = \varepsilon_0 K(k_0).\omega_s, \qquad and\ k_0 = \frac{G}{\ell} \tag{3}$$

where $K(k_0)$ is the total elliptic integral of the first kind, ε_0 is the permittivity of the free space, G is the gab of the structure, and ℓ is the length of the two parallel plates. The capacitance of the substrate layer is given by

$$\mathcal{C}_1 = \varepsilon_0(\varepsilon_r - 1)K(k_0)\,\omega_s \tag{4}$$

where ε_r is the relative permittivity of the Rogers RT5880, and h is the thickness of the substrate layer. $\mathcal{C}_0$ and $\mathcal{C}_1$ can be simplified after calculating the $K(k_0)$ approximation as follows [21]:

$$\mathcal{C}_0 = \varepsilon_0 \left(\frac{2}{\pi}\right) \ln\left(\frac{4\ell}{g}\right)\omega_s \tag{5}$$

$$\mathcal{C}_1 = \varepsilon_0 \left(\frac{(\varepsilon_r - 1)}{\frac{g}{h} + \left(\frac{4}{\pi}\right)\ln 2}\right)\omega_s \tag{6}$$

The capacitance of the two parallel plates is obtained by combining the air gap and substrate layers as follows:

$$C = \mathcal{C}_0 + \mathcal{C}_1 \tag{7}$$

According to (5) through (7), the capacitances of the proposed SSR structure can be calculated as follows: $C_1 = C_2 = C_3 = C_4 =$ 4.37 fF where $\ell = 0.85\,mm$, $g = 0.35\,mm$, $\omega_s = 0.25\,mm$, and $h = 0.254\,mm$. $C_5 = 11.5$ fF where $\ell = 0.7\,mm$, $g = 0.25\,mm$, and $\omega_s = 0.6\,mm$.

4. Results and analysis

4.1. Metamaterials losses

The new SSR structure operates at 28 GHz, which is the candidate band for future 5G. Narrow bandwidth and losses are the main impairments of the metamaterial structures, which restrict the range of their applications. At MMW regime, the inherent metamaterials losses are still a big problem and finding a low-loss structure is extremely desired. The transmission coefficient, S21, is used to measure the inherent metamaterials losses. The transmission and reflection coefficients of the simulation and equivalent circuit model of the proposed SSR structure without using reconfigurability property (no PIN diodes insert in the gaps) is shown in Fig. 4. Solid and dashed lines represent the S-parameter results of the simulation and equivalent circuit model, respectively. The SSR structure achieves a very low loss in comparison with the recent literature [22] where it is about -0.26 dB (0.96 in linear scale) at 28 GHz. The return loss and bandwidth of the proposed structure are -42 dB and 0.38 GHz, respectively. As observed from Fig. 4, the equivalent circuit model is successful in estimating the S-parameters' behavior of the SSR structure, where the simulated results agree well with the equivalent circuit results.

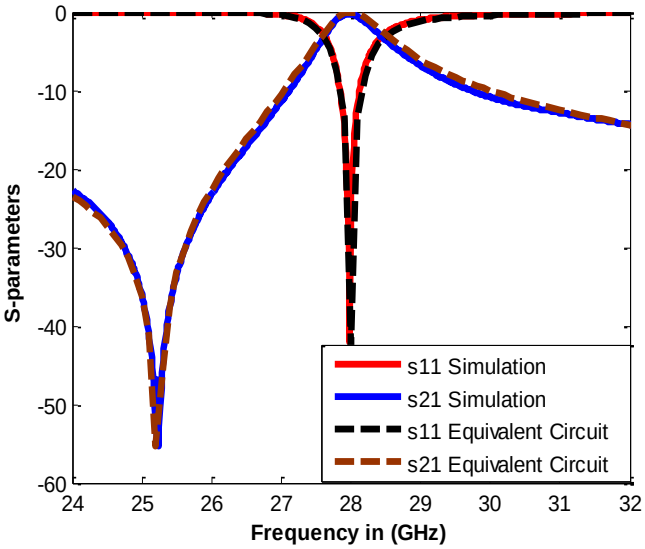

Fig. 4. The reflection and transmission coefficients of the proposed SSR unit cell. Sold lines represent the simulation results and dashed lines represent the equivalent circuit model lines.

4.2. Reconfigurable the SSR metamaterial structure

The switching property is embedded using two PIN diodes inserted in the gaps of the SSR structure. The copper strip and measured S-parameters of the proposed MA4AGBL912 PIN diode are used to achieve the configurability. Fig. 5 and Fig. 6 depict the transmission and reflection coefficients of the reconfigurable SSR structure, respectively. Solid and dashed lines represent the simulated results using the copper strip and measured S-parameters, respectively. As observed, the introduction of the high frequency switches in the gaps of the proposed structure yield different values of resonant frequencies (F1 to F3). In other words, when the state of the two PIN diodes changes between ON and OFF, the reflection and transmission coefficients are changed accordingly. From Fig. 5, it is noticeable that the SSR unit cell achieves low losses at each reconfigurable frequency for both simulation methods. As shown in Fig. 6 and Table 1, there is a mismatch in the resonant frequencies and bandwidths between the two methods that are used in the simulation. The actual MA4AGBL912 PIN diode is represented by the measured S-parameters in the simulation. Thus, the results are more accurate than another method that uses only the copper strip to represent the dimensions of the diode. Switch states and resonant frequencies of the reconfigurable SSR structure are shown in Table 1.

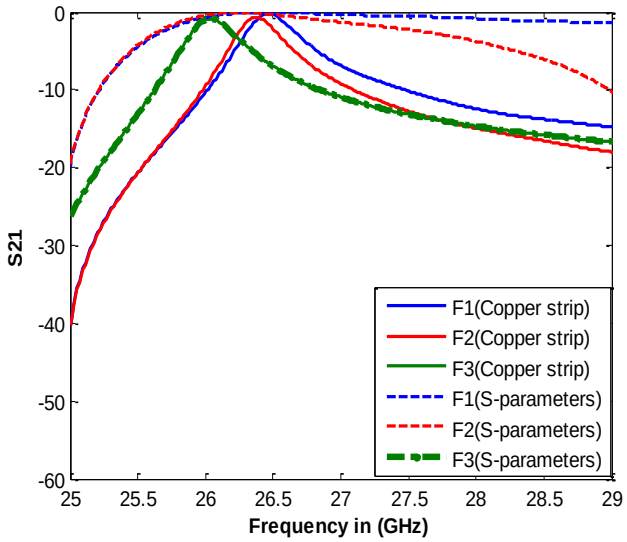

Fig. 5. Transmission coefficient of the reconfigurable SSR unit cell

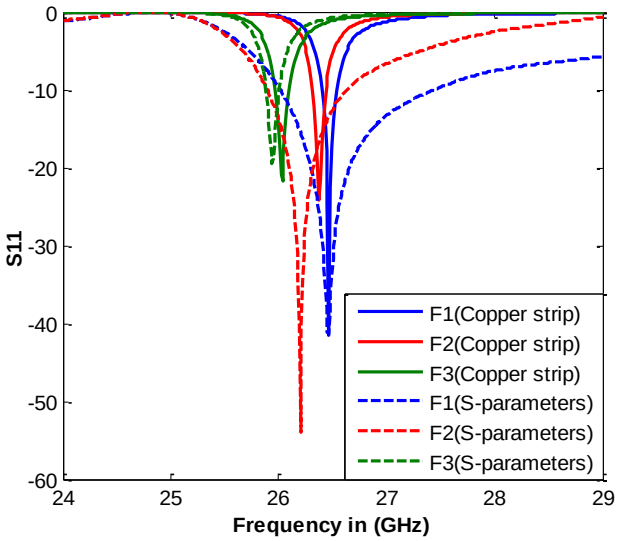

Fig. 6. Reflection coefficient of the reconfigurable SSR unit cell

Table 1. Switch states and resonant frequencies of the reconfigurable SSR metamaterial unit cell at 28 GHz

F	D1	D2	S11 (GHz)	
			Copper strip	S-parameters
F1	ON	ON	26.5	26.5
F2	OFF	ON	26.4	26.2
F3	ON	OFF	26	25.9

4.3. Negative refractive index

To retrieve the refractive index of the proposed metamaterials structure, Nicolson Ross Weir (NRW) method [23] and Robust Retrieval Method (RRM) [24] are used in this paper. In the conventional NRW method, the effective permittivity and permeability, are first computed from the complex S-parameters. Thereafter, the refractive index can be extracted using, $n = \sqrt{\varepsilon \times \mu}$. On the other hand, in the RRM, the refractive index, n and impedance, z are first obtained from the complex reflection and transmission coefficients and subsequently, the effective permittivity and permeability can be calculated. The metamaterial slab is a passive material, thus the real part of z and also imaginary part of n must be positive. The RRM is more robust and accurate than the NRW as it takes into account the signs of z and n [25].

The real parts of the effective refractive index of the SSR metamaterial unit cell without reconfiguration property are illustrated in Fig. 7. Solid and dashed lines represent the reconstructed refractive index from the simulation and equivalent circuit model, respectively. As can be seen, the double negative property of proposed structure is realized here by the negative index of refraction at the resonant frequency, 28 GHz, with about -60 for NRW method and -58 for the RRM. The retrieved refractive index results of both retrieval methods are nearly the same at the resonant frequency with percentage error of 2.5%. Furthermore, the analytical model data show good agreement with the simulated results for both retrieval methods over a whole frequency range.

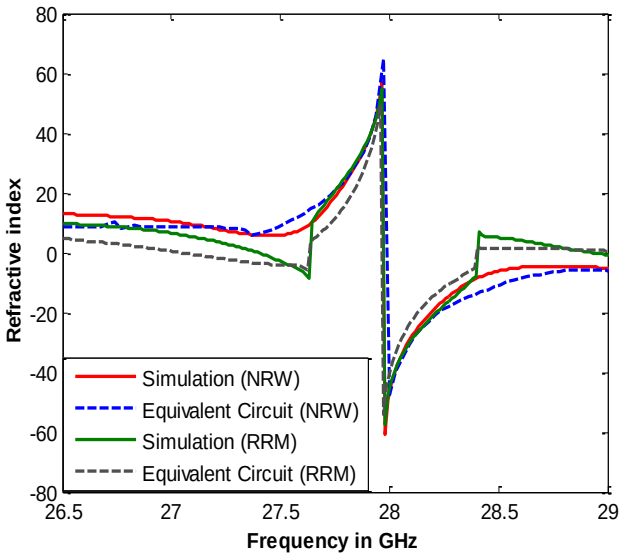

Fig. 7. Real refractive index of the SSR metamaterial unit cell without reconfiguration property using NRW and RRM methods

The real parts of the refractive index of the reconfigurable metamaterial structure for both retrieval methods, NRW and RRM, are shown in Fig. 8 and Fig. 9, respectively. It can be seen that the retrieved refractive index values are negative at the three reconfigured resonant frequencies for both methods. The switch states and retrieved refractive index values of the reconfigurable SSR unit cell at 28 GHz are described in Table 2. As shown in Table 2, when the both diodes are ON at 28

GHz, the refractive index of proposed SSR structure using NRW method is about n = -11 (copper strip) and n = -14 (S-parameters), while these values are increased to n = -9 (copper strip) and n = -12.5 (S-parameters) by using RRM method. At F2 and F3 configurations, the retrieved n values of RRM method are slightly increased over the NRW method. A noticeable increase is observed at F3 for the copper strip simulation method where the difference between the two methods is about -2. The difference in refractive index resulting from reconfigurable metamaterials can be used for future 5G beam steering applications.

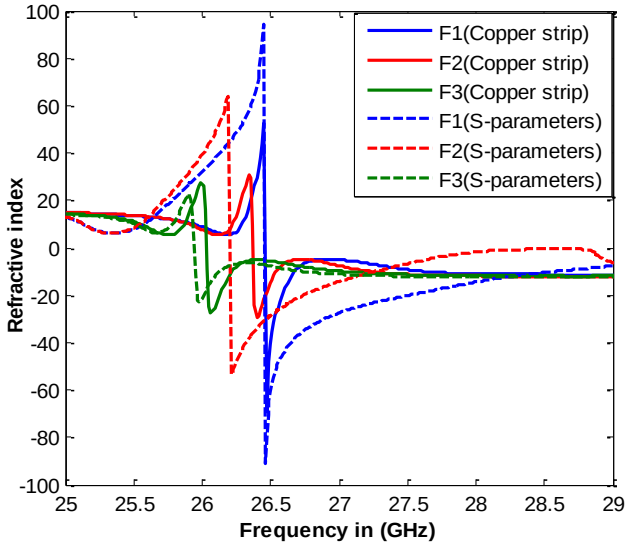

Fig. 8. Real refractive index of the reconfigurable SSR metamaterial unit cell using NRW method

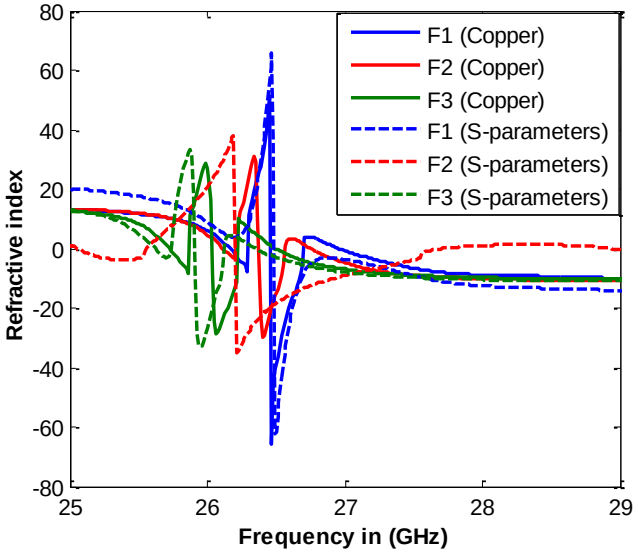

Fig. 9. Real refractive index of the reconfigurable SSR metamaterial unit cell using RRM method

Table 2. Switch states and real refractive index of the reconfigurable SSR metamaterial unit cell at 28 GHz

F	D1	D2	Refractive index, *n*			
			Copper Strip (NRW)	S-para. (NRW)	Copper Strip (RRM)	S-para. (RRM)
F1	ON	ON	-11	-14	-9	-12.5
F2	OFF	ON	-11.5	0	-10.2	1
F3	ON	OFF	-11.8	-12	-9.8	-10.4

5. Conclusion

The novel SSR metamaterial structure with a reconfigurable refractive index is presented in this paper, which operates at the future 5G band, 28 GHz, for beam steering applications. The equivalent circuit is studied and investigated to estimate the electromagnetic properties of the proposed structure. The SSR unit cell attains a low loss of –0.26 dB at a resonant frequency. The switching property is embedded using two PIN diodes positioned in the gaps of the SSR structure. The copper strip and the measured S-parameters of the proposed MA4AGBL912 PIN diode are used at the simulation stage to achieve the reconfigurability. The return loss and insertion loss at all switches states are studied and investigated. Simulation results show a mismatch in the resonant frequency and bandwidth between the two simulation methods. More accurate results are achieved using the measured S-parameters of the proposed MA4AGBL912 PIN diode. Furthermore, the real parts of the effective refractive index are investigated at 28 GHz, whereas the SSR unit cell produces a different refractive index that can be exploited to steer the antenna's main beam. The proposed structure has been validated through equivalent circuit model. This study recommends as a future work test the same structure through the fabrication and measurement.

Acknowledgments

This work was supported by Ministry of Higher Education (MOHE), Faculty of Engineering Technology, Research Center of Applied Electromagnetics, Research Management Centre, Universiti Tun Hussein Onn Malaysia (UTHM) for the support of the research under Grant No (Vote No: GPPS U735 / FRGS 1614).

References

[1] G. Deng, T. Xia, S. Jing, J. Yang, H. Lu, Z. Yin, IEEE Antennas Wireless Propag. Lett. **16**, 2062 (2017).
[2] V. Veselago, Soviet Physics Uspekhi, **10**(4), 509 (1968).
[3] J. Pendry, A. Holden, D. Robbins, W. Stewart, J. Phys. Condens. Matter **10**(22), 4785 (1998).

[4] J. Zhu, D. Li, S. Yan, Y. Cai, Q. Liu, T. Lin, EPL Europhysics Letters **112**(5), 54002 (2015).
[5] J. Soric, P. Chen, A. Kerkhoff, D. Rainwater, K. Melin and A. Alù, New J. Phys. **15**(3), 033037 (2013).
[6] J. Li, Q. Zeng, R. Liu, T. Denidni, IEEE Antennas Wireless Propag. Lett. **16**, 2030 (2017).
[7] L. Zhu, F. Meng, L. Dong, J. Fu, Q. Wu, IEEE Trans. Terahertz Sci. Technol. **3**(6), 805 (2013).
[8] B. Esmail, H. Majid, Z. Abidin, S. Dahlan, M. Rahim, International Journal of Electrical and Computer Engineering (IJECE) **7**(6), 2942 (2017).
[9] J. Turpin, J. Bossard, K. Morgan, D. Werner, P. Werner, Int J Antennas Propag. **14**, 1 (2014).
[10] T. Nesimoglu, C. Sabah, IEEE Trans. Circuits Syst. II, Exp. Briefs **63**(1), 89 (2016).
[11] B. Zarghooni, A. Dadgarpour, T. Denidni, IET Microwave Antenna P **9**(10) , 1074 (2015).
[12] R. Amiri, B. Zarghooni, A. Dadgarpour, J. Pourahmadazar, T. Denidni, Antenna Technology and Applied Electromagnetics (ANTEM), 17th International Symposium on 10 Jul, 1(2016).
[13] B. A. F Esmail, H. A. Majid, Z. Z Abidin, S. H. Dahlan, O. Ayop, M. K. Rahim, InMicrowave Conference (APMC), 2017 IEEE Asia Pacific 1325 17).
[14] P. Yasar-Orten, E. Ekmekci, G. Turhan-Sayan, PIERS Proceedings, 534 (2010).
[15] S. Ghosh, K. Srivastava, IEEE Antennas Wireless Propag. Lett. **14** , 511 (2015).
[16] V. Torres, P. Rodríguez-Ulibarri, M. Navarro-Cía, M. Beruete, Appl. Phys. Lett. **101**(24), 244101 (2012).
[17] T. Zhang, W. Xiong, B. Zhao, J. Shen, C. Qiu, X. Luo, J. Mod. Opt. **62**(11), 901 (2015).
[18] X. Xueqian Zhang, Q. Quan Li, W. Wei Cao, W. Weisheng Yue, J. Jianqiang Gu, Z. Zhen Tian, J. Jiaguang Han and W. Weili Zhang, Chin. Opt. Lett. **9**(11), 110012 (2011).
[19] M. Bueno, A. Assis, J. Phys. D **28**(9), 1802 (1995).
[20] O. Vendik, S. Zubko, M. Nikolskii, Technical Physics **44**(4), 349(1999).
[21] S. Li, W. Yu, A. Elsherbeni, W. Li, Y. Mao, Int. J. Antennas Propag. **2017**, 1 (2017).
[22] Z. He, Y. Geng, IEEE 16th International Conference on Communication Technology (ICCT), Hangzhou, China, 667(2015).
[23] O. Luukkonen, S. Maslovski, S. Tretyakov, IEEE Antennas Wireless Propag. Lett. **10**, 1295 (2011).
[24] X. Chen, T. M. Grzegorczyk, B. I. Wu, Jr. J. Pacheco, J. A. Kong, Phys. Rev. E **70**(1), 016608 (2004).
[25] J. Zhou, T. Koschny, C. M. Soukoulis, Opt. Express **16**(15), 11147 (2008).

*Corresponding author: mhuda@uthm.edu.my